Nuclear Instruments and Methods in Physics Research B40/41 (1989) 1322–1325
North-Holland, Amsterdam

Section XIII. Radiation therapy, medical and biomedical applications, neurosurgery

ANTIPROTONS FOR IMAGING AND THERAPY

Theodore E. KALOGEROPOULOS and Robert MURATORE
Physics Department, Syracuse University, Syracuse, NY 13244-1130, USA

Antiprotons are presently produced and stored at CERN and Fermilab at a rate of about 10^7 $\bar{p}$/s. Efforts are underway to develop transportable storage devices, "bottles", which would store as much as 10^{12} antiprotons for months, or years, and make the antiprotons available anywhere. A workshop held last year at the RAND Corporation assessed the science and technology of antimatter and the enabling tools. The biomedical potential of antiprotons was discussed and appears to be promising at current antimatter collection capabilities. Two applications have been studied using computer simulations: direct 3-D dE/dx imaging and the treatment of tumors with antiprotons. We discuss antiprotonic imaging and make comparisons with X-ray CT scans. The potential of antiprotons for monitoring precise delivery of radiation as well as treatment will also be discussed.

1. Introduction

Applications to medicine have been found for all stable particles known to physicists such as nuclei, photons, phonons, electrons, and positrons. The notable exception is the antiproton ($\bar{p}$) in spite of the fact that physicists have been using it since its discovery 33 years ago. The potential of antiprotons to biomedical research and medicine was recognized by Gray and Kalogeropoulos some time ago [1,2]. These pioneering investigations have been pursued further at Syracuse University with improved simulation codes and understanding [3]. The main obstacle to antiprotonic applications is the unavailability of low energy antiproton sources to users outside the high energy community.

A year ago [4], a workshop at the RAND Corporation assessed the potential of antiprotons and addressed the problem of production and accessibility. Antiprotons today are produced at Brookhaven, Fermilab and CERN. With present technology the cost of low energy antiprotons in a dedicated facility is about \$1 per 10^8 $\bar{p}$'s and as many as 10^{15} $\bar{p}$/yr can be collected [5]. Specifically, the Brookhaven AGS using the booster from pulse to pulse as an accumulator–cooler–decelerator can provide 10^{14} $\bar{p}$/yr parasitically from the slow extraction program. This would require additions to the booster and a new extraction line estimated to cost about \$10M to \$20M. To make use of these antiprotons, the antiprotons should be stored in a low energy (≤ 250 MeV) storage ring which spills them to users in a continuous manner. In such a facility biomedical research can certainly be done but the problem of the logistics of practical medical or other applications remains. The workshop addressed this question and found that it is within present technology to make transportable "bottles" in which $\sim 10^{12}$ $\bar{p}$ are stored over months or years [6]. Therefore, routine applications requiring up to about 10^{10} $\bar{p}$ are practical at present if a low energy facility were built and a transportable bottle were developed.

Various biomedical applications were discussed at the RAND Workshop [7] and were found to be possible within the antiproton source scenario outlined above. In this paper, first we overview some relevant properties of antiprotons, second we present the results of imaging simulations and compare them with actual CT scans, and third we outline the possibilities of radiation monitoring and treatment.

2. Some relevant antiproton properties

Fig. 1 gives a good overview of antiprotonic interactions in matter. The 30 in. diameter deuterium bubble chamber is about equivalent in stopping power to a 20 cm diameter water target. To a first approximation, antiprotons traversing a human head travel through about that much water. Most of the antiprotons come to rest before annihilating. In fact, the mean free path for in flight interactions in water is 21 cm. If the stopping range is 7.5 cm the fraction that stops is 70%. The antiprotons in matter behave like protons except for a larger fraction of in-flight interactions. Their difference is the annihilation.

On the average, three minimum ionizing charged pions are emitted per annihilation and most escape the human body without interaction except for multiple Coulomb scattering. In addition, an average of three gammas are produced per annihilation from π^0 decays. A few percent of these γ's interact, each producing an e^+e^- pair, one of which is seen in fig. 1. Most of the envisioned applications rely on the measurement of the annihilation point using the annihilation products, e.g., charged pions, which exit the target.

0168-583X/89/$03.50

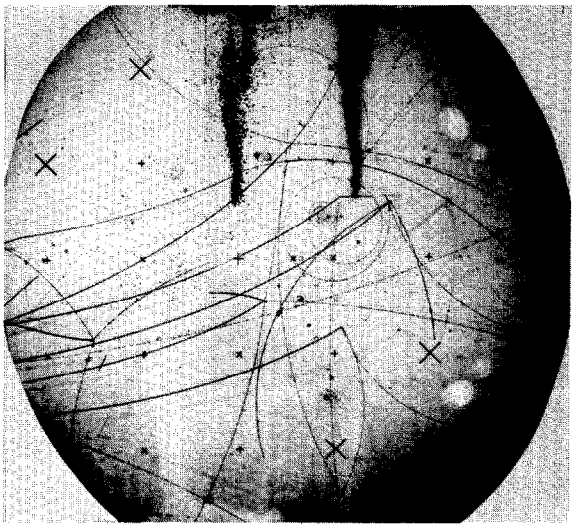

Fig. 1. In this photograph of a 30 in. diameter bubble chamber, six antiprotons entered from the left and stopped near the center. One of the antiprotons which stops near the entrance was scattered by the wall of the chamber.

Fig. 2 shows computer simulated paths followed by antiprotons in water and distributions of in-flight and at-rest annihilation vertices. The stopping antiprotons are easily discriminated from those in flight given the entering beam energy. The distribution along the beam of antiprotons annihilating at rest (fig. 2b) has a standard deviation of $0.0116R^{0.966}$ cm, where R is the range in water in cm. The distribution transverse to the beam (fig. 2c) is $\sqrt{2}$ larger. Thus for a monoenergetic pencil beam stopping at 10 cm water depth, the annihilation vertices for stopping antiprotons tend to fall within an ellipsoid 2 mm wide along the beam and 3 mm wide transverse to the beam. This precise localization is sufficient for a number of important biomedical applications.

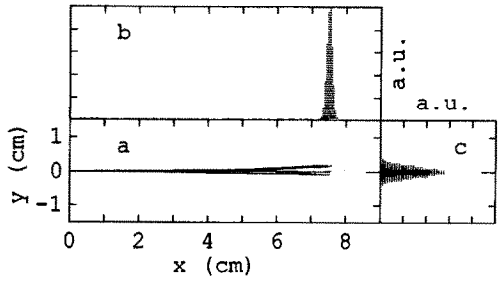

Fig. 2. A Monte Carlo computer simulation of antiprotons in water reveals the precise localization of the beam. (a) Five tracks of antiprotons originally travelling along the x-axis are projected here onto the xy-plane. The initial antiproton energy was chosen so that they would travel 7.5 cm in water on the average. (b) The annihilation vertices of a beam of 10000 antiprotons are distributed here along the beam direction. The cross hatched histogram is due to at-rest annihilations. The black histogram (almost indistinguishable from the x-axis) is due to the in-flight annihilations. The height of the histograms is in arbitrary linear units proportional to the number of annihilations. (c) The distribution of vertices transverse to the beam is broader than that along the beam.

3. Antiprotonic stereography (ASTER)

ASTER directly measures ionization or stopping power dE/dx at any point in a target. The stopping power is proportional to the density of electrons and logarithmically related to ionization potentials [7] or to elemental concentrations. Briefly, the density is proportional to $(E_1^2 - E_2^2)/(\bar{R}_1 - \bar{R}_2)$ where E_1 and E_2 are the antiproton energies upon entering the medium along the x-axis and $\bar{R}_1$ and $\bar{R}_2$ are the depths at which the antiprotons stop, respectively. To first order, this ratio is proportional to the average electronic density between the stopping points. Such measurements over the volume of interest are used for imaging. The points 1 and 2 can be as close as one wishes as long as $\bar{R}_1$ and $\bar{R}_2$ are measured with an accuracy better than $(\bar{R}_1 - \bar{R}_2)$. The error in $\bar{R}$ is

$$\sigma_{\bar{R}} = \sigma_v / \sqrt{N_{\bar{p}}},$$

where σ_v is the measuring error of the stopping point and $N_{\bar{p}}$ is the number of antiprotons. As was discussed above, $\sigma_v(\text{cm}) = 0.0116R^{0.966}$. Consequently, position resolution and density contrast along the beam are only limited by the number of antiprotons used.

Fig. 3 is a computer simulation of an ASTER scan of an 8 cm diameter Lucite disk inside a 10 cm diameter Lucite cylinder filled with water. In the 3 mm thick disk the letter E is engraved to a depth of 1.5 mm. In the simulation, this cylinder was immersed in a rectangle filled with water. The antiproton trajectories were simulated by the same program used to obtain the results shown in fig. 2. By varying the beam energy and position we obtained densities plotted in figs. 3a–3c using about 30000, 100000 and 400000 antiprotons respectively. As a comparison an X-ray CT scan was made of the cylinder in the plane containing the engraved disk and is shown in fig. 3d. We estimate that the dose due to the ASTER scan is two orders of magnitude less than that due to the CT scan.

The following are some of the important features of ASTER. (a) Imaging can be done as fast as the electronics allow. There are no mechanical movements. (b) As in photography, where the field of view is adjustable, the volume to be imaged is adjustable. Thus, one may image, for example, the eye, imparting a dose to nearby tissues orders of magnitude lower than that imparted to the imaged volume. (c) As in photography, ASTER

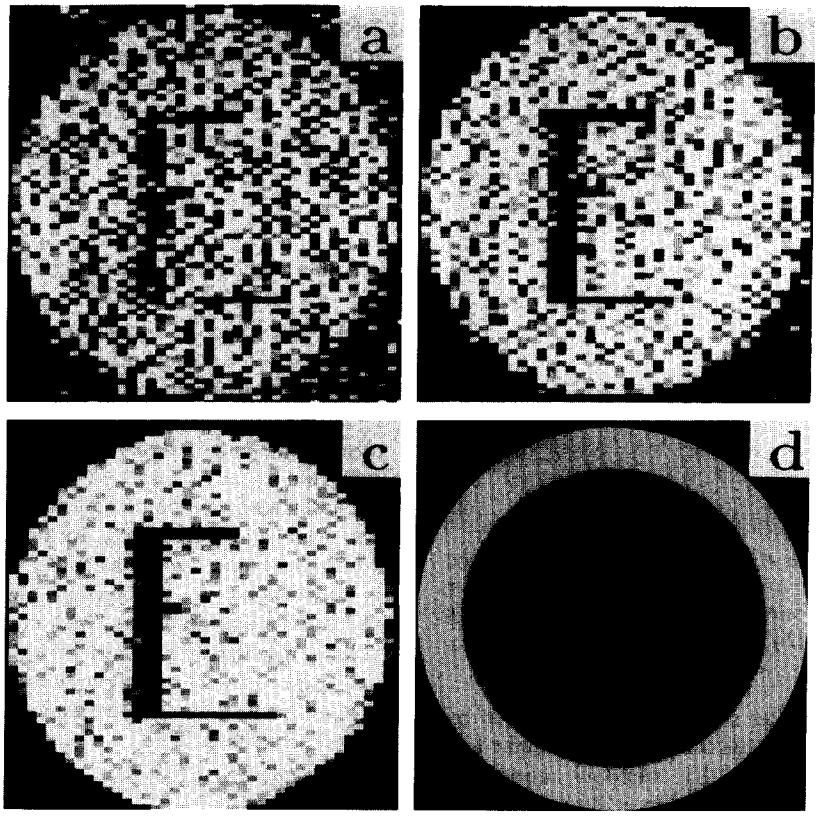

Fig. 3. ASTER produces images comparable to CT but with lower dose. (a) Simulated ASTER image of a water–Lucite phantom using about 30000 antiprotons. No "smoothing" of image has been applied. The phantom is a 3 mm thick disk of Lucite in which a 1.5 mm engraving of the letter E has been made. The Lucite disk is immersed in water. The phantom is 10 cm in diameter. Black represents a density of 1.05 g/cm^3 and white a density of 1.15 g/cm^3. (b) Like (a) but with about 100000 antiprotons. (c) Like (a) but with about 400000 antiprotons. (d) This is a photograph of an actual X-ray CT scan of the phantom described in (a). The parameters of the scan and the dose are typical of head scans.

measures *directly* the electronic density. ASTER is a 3-D "photography". (d) There are no fundamental limitations in spatial resolution along the beam or in density contrast. Practical limitations arise from the number of antiprotons. Transverse to the beam, the spatial resolution is perhaps limited by the transverse distribution of stopping vertices which is $\pm\sqrt{2} \times 0.0116R^{0.966}$ cm or at best by the vertex error.

4. Antiprotons in therapy

4.1. Simulators of therapy

The antiprotons can be used as simulators of the delivery of radiation to tumors by charged particle beams [8]. The energies required to stop charged particles at the same point depend on mass and charge. The antiproton offers the unique opportunity to measure the stopping point using a few of them by measuring their vertex and then delivering the radiation by other particles. Therefore, a bottle of antiprotons can become an indispensable calibration source to charged particle therapy installations by pinpointing the stopping point. This will drastically facilitate precise delivery of radiation.

4.2. Therapy

Antiprotons are the best particles for therapy. They have unique advantages over all other particles. First, the delivery can be extremely simple and totally under computer control. One obtains an ASTER imaging of the tumor and then delivers the radiation like taking a photograph. Second, the profile of the radiation dose delivered by antiprotons in contrast to other charged particles is better suited to therapy. In therapy one attempts to maximize the radiation delivered to a tumor and to minimize the radiation delivered to tissues outside the tumor. The radiation deposited by antiprotons

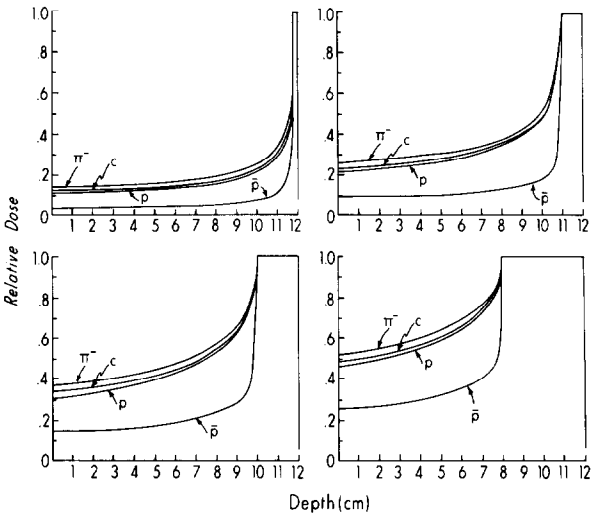

Fig. 4. Dose distributions with various (π^-, p, C, $\bar{p}$) charged particle beams are compared. In computer simulations, a uniform dose was delivered to the region of a "tumor" located at a depth of 12 cm and of variable thickness. The dose beyond 12 cm decreases rapidly and is not shown.

before annihilation is the same as that delivered by protons. In addition, the annihilation deposits about 150 MeV within a few mm of the vertex because of the heavy fragments emitted by the annihilation on nuclei. We simulated the radiation profile by antiprotons and this was found to be in agreement with measurements made at CERN by Sullivan [9]. Fig. 4 shows radiation profiles for treating tumors of various sizes. For a given dose delivered to the tumors, antiprotons deposit less than half the radiation of other particles outside the tumors. Finally, we estimate that about 10^9–10^{10} antiprotons, depending on the biological factor, are needed to treat 1 cm^3.

References

[1] L. Gray and T.E. Kalogeropoulos, IEEE Trans. Nucl. Sci. NS-29 (1982) 1051.
[2] L. Gray and T.E. Kalogeropoulos, Radiat. Res. 97 (1984) 246.
[3] A.F. DeGuzman, Ph.D. dissertation, Syracuse University (1986); R. Muratore, Ph.D. dissertation, Syracuse University (1988).
[4] Proc. of the RAND Workshop on Antiproton Science and Technology, eds. B.W. Augenstein, B.E. Bonner, F.E. Mills and M.M. Nieto (World Scientific, Teaneck, NJ, 1988).
[5] D.C. Paeslee, ibid., p. 16; Y.Y. Lee and D.I. Lowenstein, ibid, p. 39.
[6] D.B. Cline, ibid., p. 45.
[7] T. Kalogeropoulos, J. Archambeau, D. Bassano, G. Bennett, B. Gottchalk, L. Gray, A. Koehler, R. Muratore and M. Urie, ibid., p. 640.
[8] This application was discussed in an invited talk by T. Kalogeropoulos at the 2nd Int. Charged Particle Therapy Workshop, Loma Linda University Medical Center, Loma Linda, CA (1987).
[9] A.H. Sullivan, Phys. Med. Biol. 30 (1985) 1297.